Use of sky brightness measurements from ground for remote sensing of particulate polydispersions

Teruyuki Nakajima, Glauco Tonna, Ruizhong Rao, Paolo Boi,
Yoram Kaufman, and Brent Holben

The software code SKYRAD.pack for retrieval of aerosol size distribution and optical thickness from data of direct and diffuse solar radiation is described; measurements are carried out with sky radiometers in the wavelength range 0.369–1.048 μm. The treatment of the radiative transfer problem concerning the optical quantities is mainly based on the IMS (improved multiple and single scattering) method, which uses the delta-M approximation for the truncation of the aerosol phase function and corrects the solution for the first- and second-order scattering. Both linear and nonlinear inversion methods can be used for retrieving the size distribution. Improved calibration methods for both direct and diffuse radiation, the data-analysis procedure, the results from the proposed code, and several connected problems are discussed. The results can be summarized as follows: (a) the SKYRAD.pack code can retrieve the columnar aerosol features with accuracy and efficiency in several environmental situations, provided the input parameters are correctly given; (b) when data of both direct and diffuse solar radiation are used, the detectable radius interval for aerosol particles is approximately from 0.03 to 10 μm; (c) besides the retrieval of the aerosol features, the data-analysis procedure also permits the determination of average values for three input parameters (real and imaginary aerosol refractive index, ground albedo) from the optical data; (d) absolute calibrations for the sky radiometer are not needed, and calibrations for direct and diffuse radiation can be carried out with field data; (e) the nonlinear inversion gives satisfactory results in a larger radius interval, without the unrealistic humps that occur with the linear inversion, but the results strongly depend on the first-guess spectrum; (f) aerosol features retrieved from simulated data showed a better agreement with the given data for the linear inversion than for the nonlinear inversion.

1. Introduction

There have been continuous efforts in the past two decades to establish remote sensing algorithms for determining the microphysical and optical features (optical thickness, size distribution, and refractive index) of suspended aerosol polydispersions, from ground measurements of direct and diffuse solar radiation. Although such remote sensing is more informative than the traditional spectral extinction method,[1] instruments for measuring the sky radiance distribution were large in size and difficult to operate; several recent technical improvements, however, have made it possible to make very compact instruments for carrying out this kind of measurement.[2] Furthermore, satellite remote sensing of suspended matter has to be validated through ground-based measurements of aerosol characteristics.[3,4] In this situation the software used to analyze the data on direct and diffuse solar radiation for determining the columnar aerosol features becomes a bottleneck for popular utilities of scattering methods; such data have to be analyzed with techniques of inversion and radiative transfer.

To show the potential of the solar radiation measurements, we give a few examples of studies carried out before the development of the code presented in this paper; for a complete bibliography, see Ref. 5.

T. Nakajima is with the Center for Climate System Research, University of Tokyo, 4-6-1 Komaba, Meguro-ku, Tokyo 153, Japan. G. Tonna is with the Institute for Atmospheric Physics, Consiglio Nazionale delle Richerche, P. le L. Sturzo 31, 00144 Rome, Italy. R. Rao is with the Consiglio Nazionale delle Richerche, Cagliari Research Area, via Bottego 7, 09125 Cagliari, Italy. P. Boi is with the Department of Physics, University of Cagliari, via Ospedale 72, 09124 Cagliari, Italy. Y. Kaufman and B. Holben are with NASA Goddard Space Flight Center, Greenbelt, Maryland 20771. R. Rao's permanent address is the Anhui Institute of Optics and Fine Mechanics, Chinese Academy of Sciences, Hefei, Anhui 23001, China.

Received 6 March 1995; revised manuscript received 4 December 1995.
0003-6935/96/152672-15$10.00/0

As for ground-based measurements, one can refer to Shiobara *et al.*,[6] who used an aureolemeter to measure both direct solar flux and sky radiance in the almucantar, at λ = 0.369, 0.500, 0.675, 0.776, and 0.862 μm, in a suburban area of Sendai, Japan. Spectral optical thicknesses of aerosol were obtained from direct flux measurements, and aerosol size distributions in the radius interval 0.1–10 μm were estimated by inversion of both the spectral optical thickness and the angular distribution of the solar sky radiance with the algorithm of Nakajima *et al.*[1]

Examples of aureole measurements from aircraft are found in Nakajima *et al.*,[7] Tanaka *et al.*,[8] and Hayasaka *et al.*,[9] who investigated the optical properties of the tropospheric aerosol in a region of the northwestern Pacific and in an urban area around Nagoya, by means of airborne measurements of direct and diffuse solar radiation carried out with a multispectral aureolemeter; the λ = 0.332 μm wavelength was added to those used by Shiobara *et al.*[6] The results obtained concern vertical profiles of the aerosol optical thickness between the top of the atmosphere and the respective flight level, and volume size spectra of the aerosol particles in the radius interval 0.1–3 μm. The inversion algorithm of Ref. 1 was used.

The purpose of this paper is to present the software package SKYRAD.pack, which constitutes an all-in-one inversion radiative transfer package to analyze data on sky radiation for the study of the aerosol remote sensing, to illustrate the procedures for its use, to show how to calibrate the sky radiometer for both direct and diffuse radiation, to show results obtained with this code, and to discuss some connected items.

2. Definition of Observed and Computed Quantities

The solar light propagating through successive scattering processes within the atmosphere gives rise to diffuse radiation E, whereas the unscattered light constitutes direct radiation F. From ground measurements of direct and diffuse solar radiation, carried out in a cloudless atmosphere, the aerosol optical thickness, single-scattering phase function, size distribution, and complex refractive index can be derived efficiently by means of a data treatment (the SKYRAD.pack code) embodying two calibrations, an efficient radiative transfer code as well as linear and nonlinear inversion schemes.

Measurements are carried out with the sky radiometer at specified wavelengths, carefully selected outside the gas absorption bands, in order to reduce the radiative transfer problem to a pure scattering problem. One observation geometry often adopted consists of carrying out measurements in the solar almucantar, that is, pointing from the measurements' place along a conical surface with the same zenith angle θ_0 of the Sun, and letting azimuth angle ϕ vary. Another geometric situation of common use is making measurements in the principal plane, that is, pointing along a plane with the same azimuth angle of the Sun, and letting zenith angle θ vary.

The monochromatic direct solar flux density F (W m^{-2} μm^{-1}) is given by

$$F = F_0 \exp(-m_o\tau), \tag{1}$$

where F_0 is the flux at the upper limit of the atmosphere, τ is the total optical thickness, and m_o is the optical air mass that can be approximated as $m_o = 1/\cos\theta_0$ as long as $\theta_0 \le 75°$. The quantity of interest to us is τ, that is, ratio F/F_0. The monochromatic diffuse sky flux density E (in W m^{-2} μm^{-1}) is determined as the solution of the radiative transfer equation (RTE)[10]; its expression in the almucantar is given by

$$E(\theta_0, \phi) \equiv E(\Theta) = Fm_o\Delta\Omega[\omega\tau P(\Theta) + q(\Theta)], \tag{2}$$

where ω is the single-scattering albedo of the whole air mass, $P(\Theta)$ is the total phase function at scattering angle Θ, $\Delta\Omega$ is the solid view angle of the sky radiometer, and $q(\Theta)$ indicates the multiple scattering (MS) contribution. The scattering angle Θ is related to θ_0, to observation angles θ and ϕ, and to solar azimuth ϕ_0 by the expression $\cos\Theta = \cos^2\theta_0 + \sin^2\theta_0\cos(\phi - \phi_0)$ for the almucantar geometry, and by $\cos\Theta = \cos(\theta_0 \mp \theta)$ for the principal plane geometry; the $-$ or $+$ is for $\phi - \phi_0 = 0°$ or $\phi - \phi_0 = 180°$, respectively. Ranges for Θ are $0° \le \Theta \le 2\theta_0$ and $0° \le \Theta \le \theta_0 + 90°$ for the two geometries, respectively.[5]

Instead of E we consider the diffuse sky flux normalized by the direct flux, that is, the ratio

$$R(\Theta) \equiv \frac{E(\Theta)}{Fm_o\Delta\Omega} = \omega\tau P(\Theta) + q(\Theta) \equiv \beta(\Theta) + q(\Theta), \tag{3}$$

which can be measured more accurately than E and is extremely useful for long-term monitoring of the atmospheric turbidity as slightly affected by deterioration of the interference filters. Its single-scattering (SS) part equals the total differential scattering coefficient, $\beta(\Theta) \equiv \omega\tau P(\Theta)$. Equations (1)–(3) are strictly monochromatic and can be used in practice for relatively small bandpasses, in regions of the spectrum where there is not strong absorption by gases.

Figure 1 shows the behavior of ratio $R(\Theta)$ at three wavelengths and for Θ from 3° to 60°, and of the aerosol optical thickness, $\tau_A(\lambda)$, obtained from a simulation carried out with the SKYRAD.pack code; dotted curves represent the SS contribution to R. We show that the MS contribution is not negligible, and that it increases with Θ; for instance, at λ = 0.500 μm and Θ = 60° this contribution is 41%, so that an accurate scheme for the MS treatment of radiative transfer is needed within the inversion code. As for τ_A, it decreases with λ, even if other types of behavior can occur, depending on the shape of the size distribution.[12–14]

From $R(\Theta)$ data, the differential scattering coeffi-

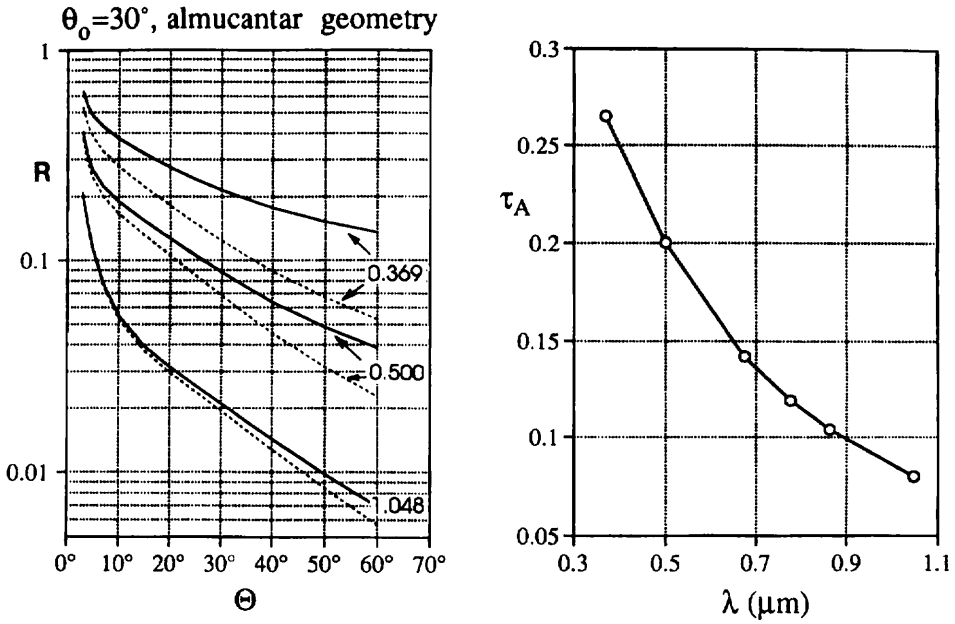

Fig. 1. Example of dependence of R on Θ, at $\lambda = 0.369$, 0.500, and 1.048 μm, and of τ_A on λ; on the left-hand side the dotted curves are the SS approximation to R. Data are from a simulation carried out with the SKYRAD.pack code, concerning the almucantar geometry and the following parameters: $\theta_0 = 30°$, $\tau_A(0.5\ \mu m) = 0.2$, ground albedo $A = 0.20$, and aerosol refractive index $\tilde{m} = 1.5–0.01i$. The aerosol size distribution was taken from Shettle and Fenn[11]; the radius interval is from 0.05 to 20 μm.

cient $\beta(\Theta)$ is obtained by an iterative regression incorporating a MS algorithm; from $\beta(\Theta)$, and possibly τ data, the volume size distribution of the atmospheric aerosol is finally derived. As the ratio R is approximately proportional to τ, the inversion procedure is very stable even for small optical thicknesses of the order of 0.01, as found in polar regions.

The aerosol optical thickness, τ_A, is defined as

$$\tau_A(\lambda) = \int_{r_m}^{r_M} \pi r^2 Q_{ext}(x, \tilde{m}) n(r) dr, \quad (4)$$

where Q_{ext} is the efficiency factor for extinction as given by the Mie theory for spherical particles, $x = (2\pi/\lambda)r$ is the size parameter, $n(r)$ is the columnar radius distribution of aerosol, r_m and r_M are minimum and maximum aerosol radii, respectively, and $\tilde{m} = m - ki$ is the aerosol complex refractive index. If in Eq. (4) Q_{ext} is replaced by the efficiency factor for scattering, one obtains the optical thickness for scattering τ_{AS}; the aerosol single-scattering albedo is defined as $\omega_A = \tau_{AS}/\tau_A$. The value of τ_A (0.5 μm) is often used as a reference parameter and is referred to as atmospheric turbidity.

The aerosol differential scattering coefficient representative of the whole atmospheric column is defined as

$$\beta_A(\Theta) = \frac{\lambda^2}{2\pi} \int_{r_m}^{r_M} [i_1(\Theta, x, \tilde{m}) + i_2(\Theta, x, \tilde{m})] n(r) dr, \quad (5)$$

where i_1 and i_2 are Mie intensity functions[10]; the aerosol phase function is defined as $P_A(\Theta) \equiv \beta_A(\Theta)/\omega_A\tau_A$.

The columnar aerosol radius distribution, $n(r)$, is the number of particles within an air column of unit cross section, for a unit radius interval (in inverse square centimeters times inverse micrometers). In the SKYRAD.pack code, columnar volume spectrum $v(r)$ is used; it is defined as the volume of aerosol for an air column of unit cross section, within a unit of logarithmic radius interval: $v(r) \equiv dV/d \ln r$ (in cubic centimeters per square centimeters). The relation between $v(r)$ and $n(r)$ is $v(r) = (4\pi/3)r^4 n(r)$.

As a consequence, the two quantities τ_A and β_A can be expressed as

$$\tau_A(\lambda) = (2\pi/\lambda) \int_{r_m}^{r_M} K_{ext}(x, \tilde{m}) v(r) d \ln r,$$

$$\beta_A(\Theta) = (2\pi/\lambda) \int_{r_m}^{r_M} K(\Theta, x, \tilde{m}) v(r) d \ln r, \quad (6)$$

where K_{ext} and K are kernel functions defined as

$$K_{ext}(x) = \left(\frac{3}{4}\right) \frac{Q_{ext}(x)}{x}, \qquad K(\Theta, x, \tilde{m}) = \left(\frac{3}{2}\right) \frac{i_1 + i_2}{x^3}. \quad (7)$$

The behavior of K_{ext} and K approximately determines the radius interval of reliable information content[15] for the aerosol optical and physical features. From the inspection of several kernels at the refractive indices typical of the atmospheric aerosol, it was found that this interval is indicatively from 0.03 to 3 μm and 0.06 to 10 μm for only extinction or scattering data, respectively; when measurements of nor-

malized diffuse sky flux are used together with the usual measurements of extinction, the radius interval is indicatively from 0.03 to 10 μm.

The aerosol refractive index is a function of wavelength; when a series of wavelengths are worked with, an average value is often assumed, possibly because of a lack of knowledge of its wavelength dependence. Besides, because the aerosol size distribution is usually multimodal, different values of $\tilde{m}$ should be properly used for each mode. Finally, we assume the aerosols are spherical particles, so that Mie theory is applied for describing the single-scattering process; in Section 6 we discuss the effect of particle nonsphericity.

3. Considerations for Instrumentation

The device used for measuring the sky radiance distribution and the direct solar irradiance is the sky radiometer, also called the aureolemeter. It is made up of a photometer with annexed interferential filters for the selection of the working wavelengths, and a pointing system; for stable measurements the center of the field of view has to have a flat response. The photometer is designed so as to have an angular field of view of 1° to 1.5°, which is suitable for measuring both the sky radiance and the direct solar irradiance. With this size, when the solar irradiance is measured, the solar disk is stably caught in the field of view, while the averaging effect on the sky radiance distribution caused by the finiteness of the field of view is almost negligible. It is important to shade the photometer with a hood that blocks the direct solar radiation for scattering angles larger than a certain value, which is also the minimum value at which the data of diffuse radiation can be reconstructed.

In our research we use aureolemeter Model Pom-01, produced by Prede (Tokyo), which adopts the following wavelengths: λ = 0.369, 0.500, 0.675, 0.776, 0.862, and 1.048 μm; all together they are referred to as standard wavelengths. In addition, the aureolemeter can operate at the 0.315-μm and 0.938-μm wavelengths for the retrieval of the optical thicknesses of ozone and water vapor, respectively. As to filters, the bandpass is less than 0.05 μm for λ = 1.048 μm and ~0.01 μm for the other wavelengths. The field of view is 1°, and the minimum angle for scattering measurements is ~3°. The photometer is mounted on a vertical–horizontal two-axes mount that is driven by digital servo motors. The measurement sequence can be controlled by a host computer, so that after latitude, longitude, date and time of the measurement site, and number and values of the aerosol scattering angles to be considered are set, several measurement modes can be programmed, such as continuous Sun photometry, aureole almucantar, and principal plane mode.

A fully automatic sky radiometer Model 318A by Cimel (Paris), used by the NASA network,[2] is worthwhile to mention in this regard. This system adopts wavelengths of 0.44, 0.52, 0.56, 0.62, 0.67, 0.78, 0.87, and 1.03 μm, with a 1.2° field of view; it is powered by solar panels and has a data-transmission system through geostationary satellites.

The quantities measured by this type of instrument are defined by Eqs. (1) and (3). We note that quantities F/F_0 and R do not need absolute radiometric calibration, so that only relative measurements have to be performed; as a consequence, if the voltage outputs for F, F_0, and E are given by V, V_0, and V_E, respectively, Eqs. (1) and (3) will be rewritten as

$$V = V_0 \exp(-m_0\tau), \qquad R(\Theta) \equiv \frac{V_E(\Theta)}{V m_0 \Delta\Omega} = \beta(\Theta) + q(\Theta). \tag{8}$$

Before τ and R actually become available for inversion, two calibrations for determination of V_0 and $\Delta\Omega$ have to be performed; the procedures for this step are described in Section 5.

A slightly different choice was made by O'Neill and Miller,[16] who developed a radiometer with a variable field of view, that is, 0.05° for measurements of direct radiation and in the solar aureole and 0.5° for scanning sky radiance outside the aureole. A different kind of instrument for measuring the sky radiance was studied by Zibordi and Voss[17,18]; it consisted of a solid-state camera with a charge injection device imaging sensor, equipped with fish-eye optics, which allows measurements over a 2π solid view angle, with an angular resolution of ~1°, in three spectral channels (0.449, 0.499, and 0.600 μm).

4. SKYRAD.pack Code

A. General Description

The code consists of two programs; the first (MKDTA) is for computing simulated data of direct and diffuse solar radiation, and the second (REDML) is for retrieving aerosol properties from solar radiation data (real or simulated). The general structure of the two programs as follows.

The MKDTA program makes simulated data of the optical quantities, for given proper input data. The main input and output data are summarized here. The input data consists of the solar zenith angle and geometry (almucantar, principal plane), the number and value of wavelengths and scattering angles, the multimodal aerosol volume radius distribution in analytical form (power law, log normal, modified gamma distribution, for each mode),[6,19] the minimum and maximum radii of aerosol particles, the aerosol complex refractive index at each wavelength, the aerosol optical thickness at one wavelength (usually 0.5 μm), and the ground albedo for each wavelength (assuming a Lambertian reflecting surface). The output data consist of the aerosol optical thickness and single-scattering albedo at the selected wavelengths, and the ratio (diffuse to direct radiation) at the selected wavelengths and scattering angles.

The REDML program retrieves the aerosol features

from data of direct and normalized diffuse radiation; its flow chart is given in Fig. 2. The input data consist of the solar zenith angle and geometry, the number and value of measurement wavelengths and scattering angles, ratios R at the above specified λ and Θ values, the optical thicknesses at the above specified λ values (if available), the ground albedo for each wavelength, the aerosol complex refractive index, and the minimum and maximum radii of aerosol particles. The output data consist of the aerosol volume spectrum, the aerosol optical thickness and single-scattering albedo at the selected wavelengths, and the aerosol phase function and reconstructed R data, at the selected wavelengths and scattering angles.

Four different modes of operation, selected by the index INDM, are available for the inversion of the optical data, according to different possible experimental conditions. In INDM = 2, the inversion entirely relies on the $R(\Theta)$ data, and only the calibration for $\Delta\Omega$ is needed. As this mode gives the results concerning v and τ_A even without calibration for direct radiation, it is very suitable for long-term measurements. In INDM = 0, the τ are kept fixed and used together with the $R(\Theta)$ data in the retrieval procedure. This mode has to have both calibrations already recalled. In INDM = 1, the τ are used as indicative values in the first step of the loop but are updated at each iteration. The τ data can be given different weights with respect to the R data, according to their reliability. In INDM = −1, the solid view angle of aureolemeter $\Delta\Omega$ is not known. The τ are used for normalizing the $R(\Theta)$ data; then the retrieval proceeds as for INDM = 0.

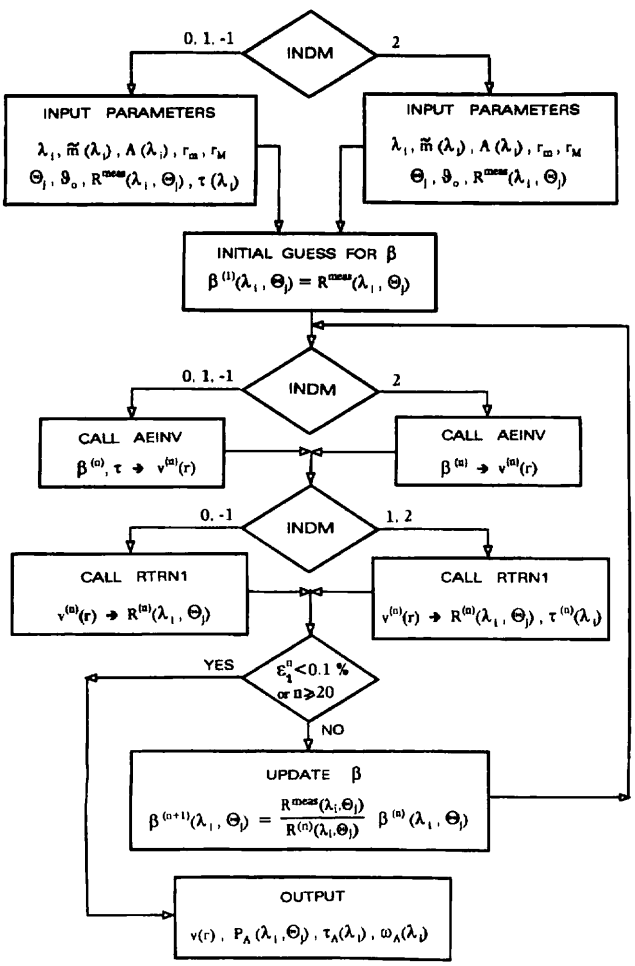

Fig. 2. Flow chart of the REDML program for inverting data of direct and diffuse solar radiation.

With reference to Fig. 2, the inversion code proceeds in this way. Starting from the initial values of $\beta(\Theta)$, at the nth iteration it computes (subroutine AEINV) $v^{(n)}(r)$ from the data of $\beta^{(n)}$ and τ (for INDM = 0, 1, −1), and then $R^{(n)}(\Theta)$ and $\tau^{(n)}$ (for INDM = 1, 2) from $v^{(n)}(r)$ through the IMS (improved multiple and single scattering) radiative transfer scheme (subroutine RTRN1); finally, it obtains $\beta^{(n+1)}(\Theta)$ by comparing $R^{(n)}(\Theta)$ with the corresponding experimental data, and then it iterates until a stop condition (maximum number of loops or the difference between successive relative residuals for R) is reached.

Mie intensity functions and efficiency factors for spherical particles are computed in advance at 55 grid points for Θ from 0° to 180°, and at 59 grid points for size parameter x (logarithmically spaced from 5.42×10^{-2} to 5.84×10^{2}); these two kinds of grid points can be chosen by the users according to their own needs, and measurement scattering angles must be on grid points. The volume radius distribution is recovered in the shape of a histogram; 20 radius subintervals within the interval from 0.01 to 10 μm are usually considered. The maximum number of iterations and the tolerance parameter for the convergence of R were set as 20 and 0.1%, respectively.

The SKYRAD.pack code has several options that can already be used or implemented over time. For instance, the inversion of $\beta(\Theta)$ and τ data can be carried out by the subroutine AEINV with a linear or a nonlinear method, according to the situation; calculations for a multilayer atmosphere can be carried out; different radiative transfer schemes can be selected; and the use of the m, k, and A input parameters as dependent on wavelength, as well as the use of different refractive indexes for the different modes of the aerosol radius distribution, can be made. Copies of the FORTRAN program are available from the first author.

B. Radiative Transfer Scheme

The connection between differential scattering coefficient $\beta(\Theta)$ and measured ratio $R(\Theta)$ occurs through the RTE in a MS scheme, which has to be both accurate and efficient in order to make the whole technique of practical use. The single-scattering theory cannot be adopted, as shown by Fig. 1 and as demonstrated, for instance, by Box and Deepak[20] and by Arao and Tanaka,[21] who showed that the SS theory for aerosols breaks down for almost all wavelengths and turbidity conditions.

Previous treatments of the sky radiance problem with a MS scheme were carried out by Weinman *et al.*,[22] Sobolev,[23] Box and Deepak,[24] and Nakajima *et al.*[1] The main part of the SKYRAD.pack code presented in this paper is composed of the IMS radiative transfer scheme in a plane–parallel atmosphere, developed by Nakajima and Tanaka.[19] The aerosol phase function is expressed, according to the delta-M method,[25] as a delta function plus a $2M$-term series of Legendre polynomials depending on Θ; this approximated phase function can be inserted into the RTE, and the procedure can be completed through a matrix formulation of the discrete ordinate method[26] for solving the transfer of solar radiation in a plane–parallel atmosphere. The radiance obtained through this procedure is not realistic, as it exhibits[19] a spike at $\Theta = 0°$ plus fluctuations around the true radiance at zenith angles smaller than 20°. On the other hand, the radiance field of a given order of scattering becomes more isotropic and smoother when the scattering order increases,[27] and the first orders of scattering dominate in the solar aureole region. As a consequence, one can remove the unrealistic features induced by the delta-M method by subtracting the approximate fields given by the first- and second-order scattering and by adding the corresponding exact estimates that are directly computed.

The exact solution to the radiance $u \equiv E/\Delta\Omega$ for the first-order scattering is given by

$$u_1(\tau, \mathbf{\Omega}) = \frac{F_0}{|\mu|} \exp(-\tau/\mu) \int_0^\tau dt \omega P(\mathbf{\Omega} \cdot \mathbf{\Omega}_0) \times \exp[(1/\mu - 1/\mu_0)t], \quad (9)$$

where $\mathbf{\Omega}$ and $\mathbf{\Omega}_0$ are unit vectors indicating the emergent and solar propagation directions, respectively; $\mu = \cos\theta$, $\mu_0 = \cos\theta_0$. The exact solution for the second-order scattering for the mean homogeneous layer is given by

$$\hat{u}(\tau, \mathbf{\Omega}) = -(1 - f\omega)\hat{\omega}^2[2\hat{P}(\mathbf{\Omega} \cdot \mathbf{\Omega}_0) - \hat{P}^2(\mathbf{\Omega} \cdot \mathbf{\Omega}_0)] \times h(\tau, \mu, \mu_0^*, \mu_0^*), \quad (10)$$

where $\hat{P}^2$, $\hat{\omega}$, μ_0^*, and h are given by

$$\hat{P}^2(x) = \frac{1}{4\pi} \sum_{n=0}^{M} (2n + 1)\bar{g}_n{}^2 P_n(x),$$

$$\hat{\omega} = f\omega/(1 - f\omega), \qquad \mu_0^* = \mu_0/(1 - f\omega),$$

$$h(\tau, \mu, \mu', \mu_0) = \frac{\exp(-\tau/\mu)}{\mu\mu'} \int_0^\tau dt \exp\left[\left(\frac{1}{\mu} - \frac{1}{\mu'}\right)t\right] \times \int_0^t dt' \exp\left[\left(\frac{1}{\mu'} - \frac{1}{\mu_0}\right)t'\right]. \quad (11)$$

In $\hat{P}^2$, terms $\bar{g}_n$ are Legendre moments of columnar-averaged phase function, P_n are Legendre polynomials, and f is the truncation fraction.

With this correction the radiances for all the emergent directions are within 1% of the true values obtained with the discrete ordinate method, with a small number of quadrature points for integrating the RTE, as shown by computations carried out for both homogeneous and inhomogeneous atmospheres with $\tau_A \leq 1$ and $\lambda = 0.500$ μm. After the internal radiances for the quadrature points are obtained, the radiances in arbitrary directions can be obtained through the Stamnes interpolation.[28] The appropriate number of Gaussian quadrature points depends on the total optical thickness and single-scattering albedo, as well as on the shape of the total phase function; in the code we chose six points, which are fast enough to be implemented into the iteration loop without noticeable error.

Note that the radiance is calculated with a scalar radiative transfer subroutine, which does not take into account polarization effects. A correction without solving the RTE for the full set of Stokes parameters is available in the SKYRAD.pack code (see Section 6).

C. Inversion Schemes

Within the SKYRAD.pack code, inversion schemes are used to derive differential scattering coefficient $\beta(\Theta)$ from measurements of normalized sky flux $R(\Theta)$, and the aerosol volume radius distribution from the data of $\beta(\Theta)$ and τ (for INDM = 0, 1, −1). The two inversions are strictly connected, as can be seen from the flow chart of Fig. 2; the inversion for β is carried out through a nonlinear method, and each step of the loop contains the procedure for retrieving $v(r)$, which consists of a single step if we adopt a constrained linear method, or even a loop if we adopt a nonlinear iterative method.

Let us recall that a nonlinear iterative method of inversion[29] starts with the assumption of a first-guess solution, which is updated at each iteration until the difference between experimental and computed data is within a prescribed value. The total differential scattering coefficient at the nth iteration is updated through the simple formula

$$\beta^{(n+1)}(\Theta) = [R^{\text{meas}}(\Theta)/R^{(n)}(\Theta)]\beta^{(n)}(\Theta); \quad (12)$$

the initial guess for $\beta(\Theta)$ is obtained as $\beta^1(\Theta) = R^{\text{meas}}(\Theta)$. If we now refer to the retrieval of $v^{(n)}(r)$ from $\beta^{(n)}$ data (INDM = 2), a nonlinear method[30,31] will give $v^{(n)}(r)$ through a loop that at the mth iteration and at the ith grid point, r_i, will update $v^{(m)}(r_i)$ with the equation

$$v^{(m+1)}(r_i) = v^{(m)}(r_i) \prod_{j=1}^{NM} (1 + \epsilon_j{}^m K_{ji}^*), \quad (i = 1, \ldots, NS), \quad (13)$$

where $K_{ji}^* = K_{ji}/K_{\max}$ is the normalized kernel, $K_{\max}$

is the maximum value of K_{ji}, and NM is the number of measurement angles. Quantity ϵ_j^m is the residual of the aerosol differential scattering coefficient for the jth angle and at the mth iteration, defined by $\epsilon_j^m = [\beta_j^{(n)}/\beta_j^{(m)}] - 1$, with $\beta_j^{(m)}$ computed by the use of $v^{(m)}(r_i)$, $(i = 1, \ldots, NS)$. The estimation of the first-guess solution is particularly important, as it allows us to speed up the convergence of the solution; for the first-guess spectrum the sum of three log normals was assumed, whose parameters are fixed according to the situation.

The constrained linear method of inversion[29] consists of a linear matrix formulation in which the stability of the solution is controlled by the requirement that it agree both with input data and with imposed weighted constraints. With reference to the retrieval of $v^{(n)}(r)$ from $\beta^{(n)}$ and τ data (INDM = 0, 1, −1), the system of equations can be expressed in a matrix equation as

$$\mathbf{g} = \mathcal{A}\,\mathbf{v}^{(n)} + \boldsymbol{\epsilon}, \tag{14}$$

where $\mathbf{g}$ is the vector of the $\beta_A^{(n)}$ and τ_A data, $\mathbf{v}^{(n)}$ is the unknown vector of components $v^{(n)}(r_i)$, the components of vector $\boldsymbol{\epsilon}$ are the error of each datum, and matrix $\mathcal{A}$ is composed of the kernel elements. By introducing a smoothing matrix $\mathcal{H}$ and a Lagrange multiplier γ,[32–34] which constitutes a relative weight between $\mathcal{A}$ and $\mathcal{H}$, we obtain the solution

$$\mathbf{v} = (\mathcal{A}^T\mathcal{A} + \gamma\mathcal{H})^{-1}\mathcal{A}^T\mathbf{g}, \tag{15}$$

where $\mathcal{A}^T$ is the transpose of $\mathcal{A}$. In the SKYRAD.pack code, parameter γ is found according to the method of Ref. 35.

Advantages of nonlinear over linear methods consist[29] of the following: (a) the iterated nonlinear solutions are always positive, whereas unrealistic humps in the retrieved spectrum can be produced by the linear inversion; (b) the nonlinear inversion gives satisfactory results in a larger radius interval; (c) it is more simple to be coded; and (d) it is less susceptible to noise.

Figure 3 shows the volume spectra retrieved from the R data of Fig. 1 (mode INDM = 2), with a linear and a nonlinear inversion scheme, by the use of the SKYRAD.pack code. We show that for the linear inversion the relative difference, Error (%), between given and retrieved size distributions as a function of r increases toward both sides of the assumed radius interval (0.05–20 μm), reaching values near 60% at the limits; the nonlinear inversion extends the reliable interval on both sides of the interval. If we consider as reliable those radii for which Error (%) ≤ 25%, the radius intervals concerning the linear and the nonlinear inversion will be 0.75–11 μm and 0.6–18 μm, respectively. A similar effect is obtained by the use of both data of extinction and scattering, as shown by Fig. 4, where volume spectra retrieved from the data of Fig. 1, for INDM = 0 and INDM = 2, are reported; we note that use of the mode INDM = 0

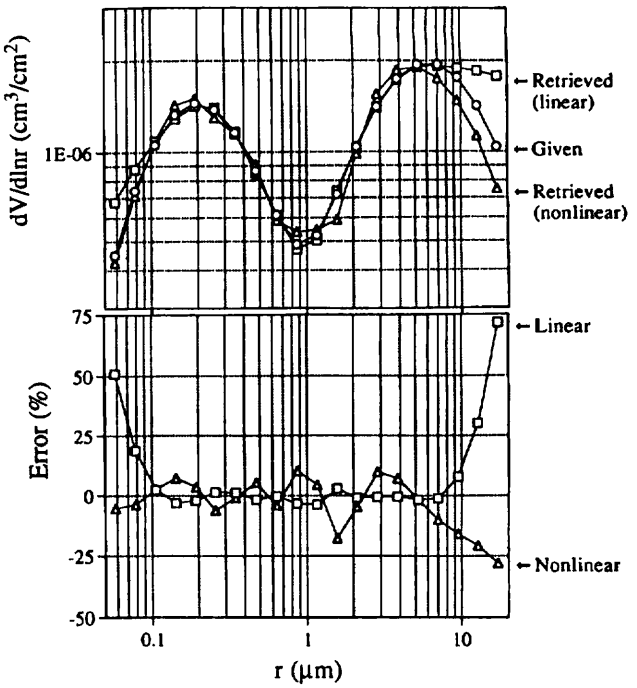

Fig. 3. Aerosol volume size distributions retrieved with a linear and a nonlinear inversion scheme from the ratios R of Fig. 1 (mode INDM = 2), within the $3° \le \Theta \le 30°$ interval; at the bottom there is the relative difference between given and retrieved spectra. The inversion was carried out with the SKYRAD.pack code, assuming a radius interval from 0.05 to 20 μm.

allows us to improve the radius resolution, mainly on the side of smaller radii (from 0.75–11 μm to 0.6–14 μm).

To study the features of the linear and nonlinear inversions within the SKYRAD.pack code further, we carried out simulations with six types of spectra, under the conditions τ_A (0.5 μm) = 0.2, $A = 0.1$, $\tilde{m} = 1.5 - 0.01i$, $r_m = 0.01$ μm, and $r_M = 20$ μm. The reliability of the findings was assessed through the following control parameters: $\epsilon(v)$, the average of Error (%) over the radius subintervals that contribute more than 5% in reconstructing any optical quantity[5]; $\epsilon(\tau_A)$, the relative deviation between simulated and retrieved aerosol optical thicknesses; and $\epsilon(R)$, the rms deviation between simulated and reconstructed R data, averaged on the scattering angles. Results from R data (INDM = 2) showed that $\epsilon(v)$, $\epsilon(\tau_A)$, and $\epsilon(R)$ are always smaller for the linear inversion, whereas the nonlinear inversion gives satisfactory results in a relatively wider radius interval, without the unrealistic humps in the spectrum typical of the linear inversion; the results coming from the nonlinear inversion showed a strong dependence on the first-guess spectrum.

From the elaboration of both simulated data and measurements taken in the center of the Mediterranean Sea, Cagliari, Sardinia, we saw that computational times for the two methods were almost the same (~30 s on the workstation HP Apollo 9000), because the nonlinear method has to iterate, whereas

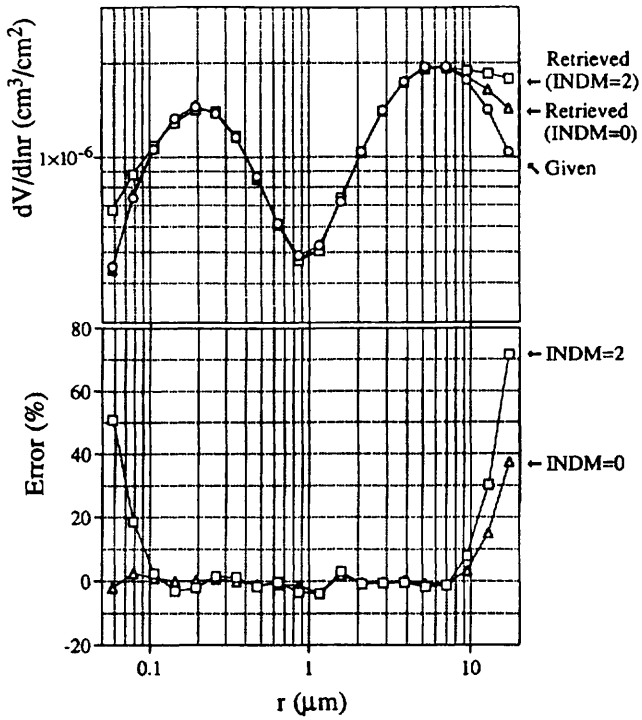

Fig. 4. Aerosol volume size distributions retrieved with the SKYRAD.pack code, for modes INDM = 0 and INDM = 2, and the linear inversion method; at the bottom there is the relative difference between given and retrieved spectra. Data are from Fig. 1, with R within the $3° \le \Theta \le 30°$ interval; a radius interval from 0.05 to 20 μm was assumed.

the linear method has to invert the matrix in Eq. (15) and perform several trials to find the best estimate of the γ parameter.[35]

5. Calibrations and Data-Elaboration Procedure

The determination of quantities R and τ requires us to determine previously $\Delta\Omega$ and V_0 in Eqs. (8); we propose two methods for these calibrations, that is, the Sun scanning method and an improved version of the Langley plot, respectively.

The inversion of the optical data requires knowing or determining the input parameters, so we propose a procedure of inversions that also determines m, k, and A averaged over wavelength; this procedure is connected with the calibration for V_0, as shown below. Both calibrations and the data-elaboration procedure are at present under investigation.

A. Determination of the Solid View Angle

There are several possible ways of determining the solid view angle of the radiometer. For instance, the lamp method[2,3] consists of looking at a uniform target with known brightness as an integrating sphere with well-calibrated standard lamps. The solid view angle is then given by

$$\Delta\Omega = E/c\bar{L}, \tag{16}$$

where $\bar{L}$ is the mean radiance for the field of view, E is the diffuse flux density, and c is a constant; this calibration requires a careful maintenance of the light source and integration sphere. The diffuse-plate method consists of first looking vertically at the solar disk and then horizontally at a diffuse plate illuminated by the direct solar radiation and placed at 45° with the vertical direction. If we know the flux reflectance, r, of the diffuse plate and assume isotropic reflection at its surface, the solid view angle will be given by

$$\Delta\Omega = \pi E/rcF. \tag{17}$$

The point-source method[7] uses a plane–parallel light source, such as a collimated lamp, to measure the response function of the radiometer field of view. In this paper we propose using the Sun as a plane–parallel source of radiation, centered at the origin of a local system of rectangular coordinates (x, y); the method consists of scanning a small domain ΔA around the Sun. In this case the solid view angle is calculated as

$$\Delta\Omega = \iint_{\Delta A} E(x, y)\mathrm{d}x\mathrm{d}y/E(0, 0) \equiv \iint_{\Delta A} f(x, y)\mathrm{d}x\mathrm{d}y, \tag{18}$$

where $E(x, y)$ is the diffuse flux density when the optical axis of the radiometer is located at (x, y), and $f(x, y)$ is the response function of the radiometer. We estimated the solid view angle of an aureolemeter Model Pom-01 L (Prede) with this method, by scanning the area of $2° \times 2°$ around the solar disk from up to down and from left to right, with an angular resolution of 0.1°; measurements were made for all seven channels of the radiometer. After we corrected for the movement of the solar disk during the scanning procedure, we registered the signals as a function of the (x, y) coordinates system. Finally, to obtain the integral in Eq. (18), we introduced an elliptic system of coordinates centered at (0, 0), so that the response function was expressed as a function of ellipse major semiaxis r, $f(x, y) \equiv f(r)$, as shown in Fig. 5 for $\lambda = 0.500$ μm. The values of $\Delta\Omega$ are near 2×10^{-4} sr and decrease with wavelength because of the color aberration of the single lens used in the radiometer. In the above discussion we assumed the solar disk as infinitely small, whereas it has an angular radius of ~0.23°; this effect will not change Eq. (18) as long as the solar disk is smaller than the flat part of the center of the field of view.

B. Calibration of Direct Radiation Measurements

The usual method for finding V_0 uses the Langley plot,[36,37] which is based on measurements of only direct radiation, and which for each wavelength locates V_0 on a $V - m_o$ graph for $m_o \to 0$, under the hypothesis that τ is a constant during the calibration. Because measurements last several hours, the above hypothesis is almost never fulfilled, so the accuracy of $V_0(\lambda)$ is often poor; a simulation carried out by

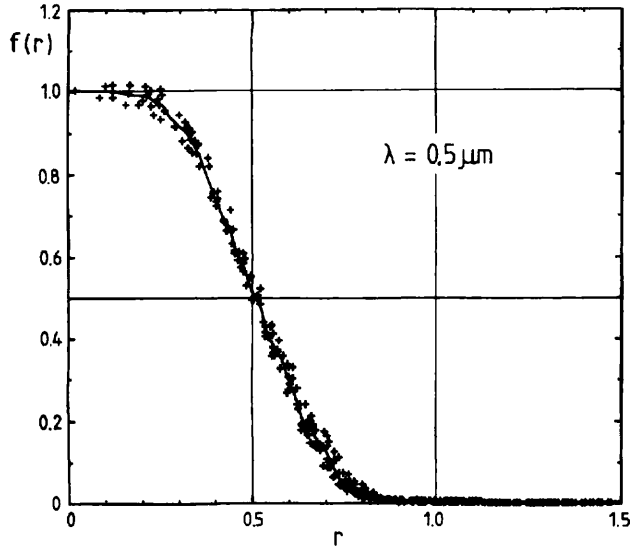

Fig. 5. Method solar disk scanning for the determination of the solid view angle of the sky radiometer. Behavior of the response function versus r, from measurements concerning aureolemeter Model Pom-01 L (Prede); $\lambda = 0.500$ μm.

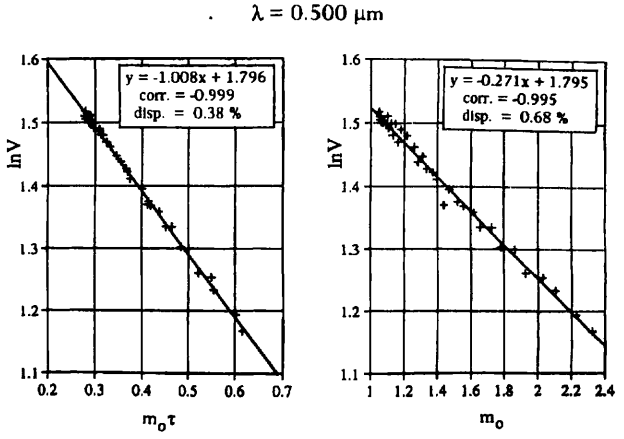

Fig. 6. Left-hand side shows the improved Langley plot; optical thicknesses were derived from R data (INDM = 2), with input parameters $m = 1.4$, $k = 0.01$, $A = 0.1$. The right-hand side shows the normal Langley plot. Experimental data were taken in the center of the Mediterranean Sea, Cagliari, Sardinia, and elaborated with the SKYRAD.pack code.

Shaw[38] for an urban situation in the midvisible showed V_0 to have an error of ~10%.

Here we propose an improved method of calibration based on data concerning both direct and diffuse radiation, which is an extension of a previous method by Tanaka *et al.*[39] A retrieval with only R data (INDM = 2) is performed for all available measurements, and the set of τ values so obtained is used for deriving $m_o\tau$ and then V_0 by extrapolation along a $V - m_o\tau$ graph, as required by the first of Eqs. (8). The values of V_0 determined with this method depend on the input parameters assumed when the mode INDM = 2 is entered; at present, the input parameters were assumed to be averaged over wavelength.

Figure 6 shows an improved and a normal Langley plot at $\lambda = 0.500$ μm, obtained from experimental data taken in Cagliari, Sardinia, at the standard wavelengths. We show that the improved Langley plot gives a better correlation coefficient and a smaller dispersion of the points about the best-fit line; the same holds for the other wavelengths, mainly at the longer ones. In this case the relative difference of the normal V_0 from the improved one is less than 0.1%; for all the wavelengths considered we have 1.1, −0.06, −0.6, −0.8, −0.9, and −0.9%, respectively. For other measurements carried out almost at the same site, we obtained differences of approximately 3%. The corresponding improved V_0 values for the two cases were closer to each other than the normal values. Furthermore, we have to take into account that according to the first of Eqs. (8) an error on V_0 propagates on τ according to

$$\frac{d\tau}{\tau} = \frac{1}{m_o\tau}\frac{dV_0}{V_0}, \tag{19}$$

and that for our experimental data $1/m_o\tau$ varies in the intervals 0.6–1.4, 1.6–3.6, 3.2–7.1, 4.1–9.3, 4.8–11.4, and 5.6–14.3 for the wavelengths considered; as a consequence, a 1% error on V_0 can easily imply an error of 10% or more on τ.

C. Data-Elaboration Procedure

In addition to the data elaborated for the present paper, the SKYRAD.pack code was used in several cases, both with simulated and measured data. Tonna *et al.*,[5] starting from nine models of atmosphere characterized by parameters θ_0, A, and τ_A (0.5 μm) and by the measurement geometry, computed optical data at the standard wavelengths, which were subsequently inverted to recover the aerosol volume spectrum; the retrievals were carried out for all four available modes (index INDM), using R data in the $3° \le \Theta \le 30°$ interval. The aerosol spectra considered for this study were the bimodal volume spectrum of Shettle and Fenn[11] already used for producing the data of Fig. 1, and a bimodal spectrum retrieved by Shiobara *et al.*[6] that had a radius interval from 0.1 to 10 μm; refractive indices for the two spectra are 1.48–0.055i and 1.50–0.01i, respectively. Results showed that $\epsilon(R)$ is within 0.3% for all modes, whereas $\epsilon(\tau_A)$ is within 0.3% and 1.5% for INDM = 0, 1, −1 and INDM = 2, respectively. We note that these results turned out to be very good, as before starting the inversion, we assigned for input parameters r_m, r_M, m, k, and A their true values, that is, the same values used in simulating the measurement data. When actual field data are retrieved, these parameters are unknown.

Kaufman *et al.*[40] carried out ground measurements of solar transmission and sky radiance in several geographical regions by means of a combined Sun photometer–radiometer operating at eight spectral bands from 0.44 to 1.03 μm for direct sunlight, and at three spectral bands (0.44, 0.62, and 0.87 μm) for sky radiance measurements. The angular depen-

dence of the almucantar sky radiance in the interval $2° \leq \Theta \leq 40°$ was used to retrieve with the SKYRAD.pack code the aerosol size distribution in the radius interval $0.06 < r < 10$ μm; bimodal and trimodal volume spectra were found, which depended on the measurement site. Aerosol optical thickness τ_A was determined both from data of direct radiation by the use of a normal Langley plot and from only R data with INDM = 2. In the elaboration, characteristic values for the input parameters were assumed.

Kaufman *et al.*[41] produced average volume size spectra derived from 160 measurements of sky radiance from ground, collected in the easter U.S. during the SCAR-A (sulfates cloud and radiation—Atlantic) experiment in 1993, which are reported in Fig. 7. Four main modes of aerosol can be distinguished in this set of spectra: the accumulation mode ($r < 0.3$ μm), the stratospheric aerosol mode ($0.3 < r < 0.8$ μm), the maritime salt particles mode ($0.8 < r < 2.5$ μm), and the coarse particles mode ($r > 2.5$ μm). In the elaboration the SKYRAD.pack code was used; characteristic values for the input parameters were assumed.

Dalu *et al.*[42] carried out ground measurements of optical, chemical, and physical properties of aerosol in Sardinia, Italy, with a Model Pom-01 aureolemeter, an advanced Sun photometer, and cascade impactors. Optical data were elaborated with mode INDM = 2 in the $3° \leq \Theta \leq 35°$ interval, by the use of the SKYRAD.pack code. The obtained aerosol spectra indicated a trimodal volume size distribution, with mode radii located at approximately 0.15, 0.5, and 2 μm, which were related to background aerosol, maritime, and sea salt particles, respectively. The diurnal behavior of τ_A was also determined. Many sets of values of the refractive index and ground albedo were selected for the computations, and an optimal set averaged over wavelength was determined at each hour from the minimum shown by residuals

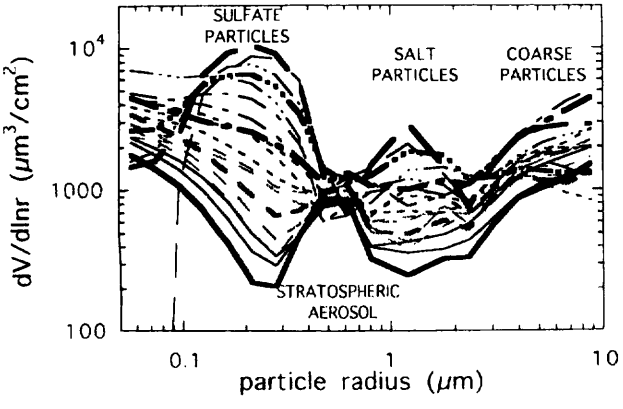

Fig. 7. Aerosol volume distributions derived with the SKYRAD.pack code from sky measurements by Sun/sky radiometers during the SCAR-A experiment; data are averaged every 5 or 10 measurements. For radius $r < 0.3$ μm, accumulation mode; $0.3 < r < 0.8$ μm, stratospheric aerosol mode; $0.8 < r < 2.5$ μm, maritime salt particles mode; $r > 2.5$ μm, coarse particles mode.

$\epsilon(R)$. Residuals $\epsilon(R)$ were found to depend rather strongly on m and only weakly on k and A; for r_m and r_M the fixed values 0.01 and 10 μm were assumed.

The problem concerning the sensitivity of the results to and the dependence of control parameter $\epsilon(R)$ on the input parameters was studied in Ref. 5. Using the same models of atmosphere as those given in the first paragraph of this subsection, Tonna *et al.*[5] demonstrated that inaccurate values of the input parameters can cause great errors in the results, while the dependence of $\epsilon(R)$ can be very weak. Data were elaborated for mode INDM = 2 at the standard wavelengths by the use of the SKYRAD.pack code. Results can be summarized as follows. First, the effect of selecting r_m and r_M values different from the true ones is that the results concerning v and τ_A deteriorate, whereas $\epsilon(R)$ practically does not vary; the best result for each case is obtained when the assumed radius interval is slightly larger than the original one. The interval $0.05 \leq r \leq 15$ μm was shown to be a reasonable compromise. Second, as to the ground albedo, when A departs from the true value the results of the inversion concerning v and τ_A rapidly deteriorate, while $\epsilon(R)$ practically does not vary; if we want to keep $\epsilon(\tau_A)$ within 5%, we have to determine A within 15%. Third, as to the aerosol complex refractive index, when m departs from the true value the results of the inversion concerning v and τ_A rapidly deteriorate, while at the same time $\epsilon(R)$ shows a clear minimum about the true value; if we want to keep $\epsilon(\tau_A)$ within 5%, we have to determine m within 3.5%. Furthermore, when k departs from the true value, v and τ_A rapidly deteriorate, while $\epsilon(R)$ shows a very weak dependence on k; if we want to keep $\epsilon(\tau_A)$ within 5%, we have to determine k within 20%.

Instead of determining the above parameters from additional measurements,[43–45] we conceived of deriving them from the optical data by using the $R(\Theta)$ data in their entire possible angular range rather than on a restricted interval of Θ values. By taking into account that $R(\Theta)$ depends differently on the various parameters within different Θ intervals, one can divide the $R(\Theta)$ data into two or three sets, and within each data set one can search for the proper parameter. Figure 8 shows the dependence of R on m, k, and A, at $\lambda = 0.500$ μm, in the Θ interval from 3° to 160°, which is the widest that can actually be used for measurements; data were generated with the MKDTA program enclosed in the SKYRAD.pack code by the use of an aerosol spectrum by Shettle and Fenn.[11] More specifically, Fig. 8 (top left) shows $R(\Theta)$ for four values of m, for given k and A; it can be seen (right) that the Θ interval of maximum variation with m is from 3° to 30°, while at the same time (middle and bottom) within this interval the minimum dependence of R on k and A occurs. As to the variation of R with k, Fig. 8 (middle right) shows that it is almost constant from 30° to 160°, while (bottom right) a maximum in the variation of R with A occurs from 90° to 120°.

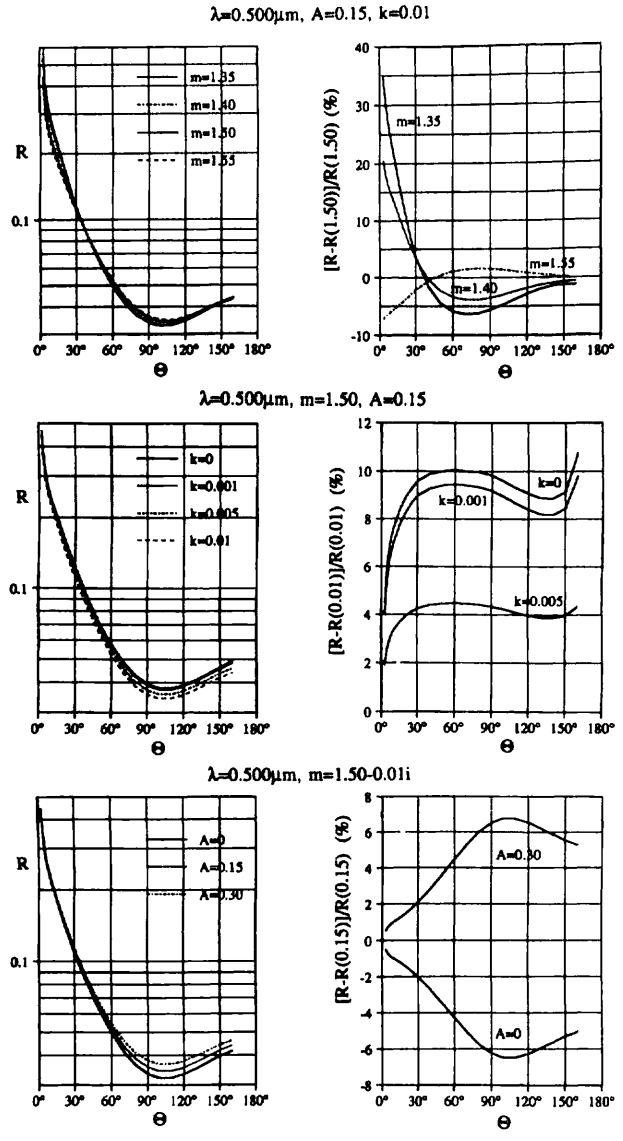

Fig. 8. Dependence of $R(\Theta)$ on m (top), k (middle), and A (bottom). Data are from numerical computations carried out with the SKYRAD.pack code and refer to an aerosol volume radius distribution by Shettle and Fenn.[11]

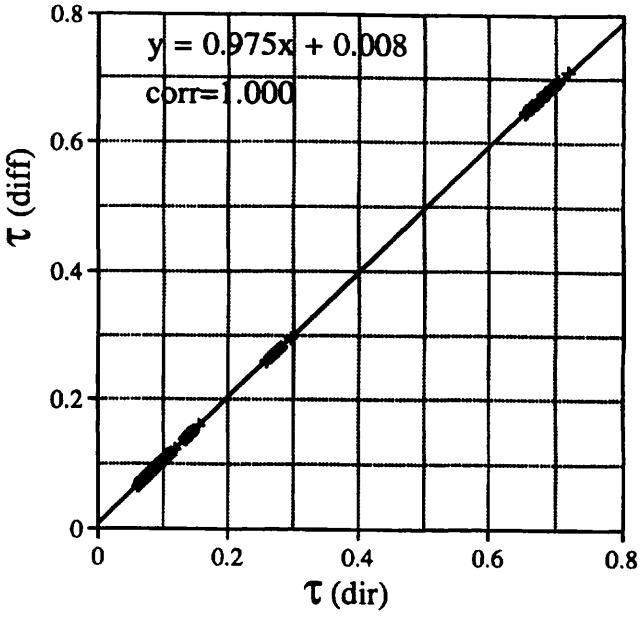

Fig. 9. Comparison between optical thickness [τ(dir)] derived from Sun photometric data with improved Langley plots and [τ(diff)] derived from diffuse light data; results from all the six standard wavelengths were put together. Experimental data are as in Fig. 6, elaborated with the SKYRAD.pack code.

On the basis of all the above findings, we created the following inversion procedure. Let us suppose that we carried out measurements of both direct and diffuse radiation during a whole day, so as to have ~30 complete sets of measurements. After determining $\Delta\Omega$, we invert each set of data with mode INDM = 2 in the interval $3° \le \Theta \le 30°$, assuming about six values of m and indicative values for k and A; from the minimum exhibited by $\epsilon(R)$, the average over wavelength, with m, we can determine m, taking advantage of the fact that the dependence of $\epsilon(R)$ on k and A is very weak for the considered Θ interval.

Now elaborate each set of data with INDM = 2, assuming approximately six values for k, the above determined m value, and an indicative value for A. For each couple of k and A values, construct the improved Langley plot by fitting the straight line $\ln V = \ln V_0 - cm_o\tau$ for each wavelength; from the minimum exhibited by deviation $\epsilon(c) \equiv (c - 1)$, the average over wavelength, with k, we can determine k, as well as the best estimate of the set of V_0 values.

By means of the best V_0 values found, we can now derive τ from measurements V of direct reading. As a check of the quality of the measurements, calibrations, and inversion procedure, aerosol optical thickness τ(dir) derived from measurements of direct radiation was compared with optical thickness τ(diff) retrieved from sky radiance data. Figure 9 shows the behavior of τ(diff) versus τ(dir) for measurements carried out in Cagliari, Sardinia, with the above procedure; data from all six standard wavelengths were put together. The offset of 0.008 is probably due to an error in the calibration of direct reading,[40] whereas the 0.975 value in the slope should come from an error in the value of the solid angle. Besides, we know from Fig. 8 that for Θ within the 90°–120° interval, R shows a strong dependence on A; this suggests that we reconstruct R in this Θ interval by means of the results previously obtained, and that we try to find a better value for A from the minimum exhibited by $\epsilon(R)$ with A. Finally, a further step could be to use the τ(dir) and R data, together with the average input parameters so far determined, for entering mode INDM = 0 and getting final results.

6. Conclusions and Remarks

Results from both simulations and experimental data showed that the SKYRAD.pack code can retrieve the optical and microphysical features of the colum-

nar atmospheric aerosol with accuracy (within 1% of the measured optical quantities) and efficiency (within 30 s) in several different situations, provided that the pertinent input parameters are properly given. Within the scheme proposed, absolute radiometric calibrations of the sky radiometer are not needed. New and improved methods for performing the two calibrations for $\Delta\Omega$ and V_0 have been discussed, which can be carried out with field data.

A procedure of inversion including the above calibrations was proposed; it makes use of all the information contained within the optical quantities and also determines average values for the three input parameters m, k, and A. We note that besides their proper physical meaning, m, k, and A can be also considered as adjustment parameters, because they partially absorb the effects that cannot be reliably introduced into the model (i.e., nonsphericity of aerosol particles, nonhomogeneity of the surface around the measurement site); furthermore, they also depend on the inversion model used for their determination from measurements,[46] so they can be ultimately referred to as apparent or effective parameters. The procedure of inversion is still under investigation with both simulated and experimental data.

The above procedure was not conceived to find input parameters r_m and r_M, which condition both the accuracy of the results and the shape of the retrieved spectrum in a rather irregular way. At present, in the SKYRAD.pack code we use fixed values for these parameters[5] of 0.05 and 15 μm, respectively.

Simulations carried out with the LOWTRAN 7 code, for a midlatitude standard atmosphere characterized by an aerosol turbidity of 0.2, showed that the contribution of the optical thickness caused by the atmospheric gases to the total optical thickness is 0.0%, 2.8%, 6.3%, 0.2%, 1.6%, and 1.8% for the six standard wavelengths. In an Antarctic atmosphere with a turbidity of 0.02, the above contributions, for the six wavelengths, becomes 0%, 5.8%, 19%, 0.7%, 2.5%, and 8%, respectively. In this situation gas absorption could have some influence on the measured values of R and τ, and consequently on the final results of the inversion. As to R, absorption partly compensates in the ratio, as it will affect the diffuse and direct flux densities by nearly the same fraction, so that we believe that the ratio R can reliably be used without correction at the standard wavelengths, while a correction can be done on τ. To this end, we have to find both constant V_0 in the first of Eqs. (8) in the presence of gaseous absorption and the gas optical thickness,[36,38] which can be done, for instance, with the method set up by Reagan *et al.*[47]

In the SKYRAD.pack code the aerosol particles are assumed to be homogeneous spheres. The effect of particle nonsphericity on the retrieval of the aerosol size distribution from scattering data was examined, for instance, in Ref. 48.

Although there are several theories for calculating the light-scattering properties of nonspherical particles,[49–50] efficient computational codes like those for spherical particles[52] are not available. Besides, the semiempirical theory of Pollack and Cuzzi[53] was found by both Asano and Sato[49] and by Mugnai and Wiscombe[50] to disagree with their results; this finding was ascribed to a lack of solid theoretical grounds.

With measurements carried out with a polar nephelometer, Nakajima *et al.*[54] showed that the aerosol nonsphericity can be taken into account by means of a large fictitious absorption. The consequence of this result on the actual use of the SKYRAD.pack code is that should an unusually great value of k be determined, one could think of a possible effect of particle nonsphericity.

Because of the finite acceptance angle of the optical receiving system, the Sun photometer also collects a fractin of diffused light, in contrast with the hypothesis implied in Eq. (1). This effect was studied by some authors.[38,55,56] We note that even if the error in F is generally agreed to be within a few percent, the error implied in τ can be greater, as observed for V_0 in Subsection 5.B., Eq. (19).

Actual corrections to τ were provided by Shiobara and Asano[57] and by Nakajima *et al.*[58] The latter authors[58] proposed a correction to Eq. (1) that was based on a perturbative scheme developed by Box and Deepak[24] as a solution to the RTE. We note that an analysis of this problem close to that proposed in Ref. 58 was carried out by Box and Deepak.[59] This effect will be included in the SKYRAD.pack code.

Calculations of sky radiance for clear and turbid atmospheres, carried out with formulations neglecting polarization effects, involve systematic errors[60] up to ~10%. A technique for reducing these errors is described in a paper by Ogawa *et al.*,[61] in which the true sky radiance is divided into two parts, i.e., that calculated by the use of the scalar approximation and an additional sky radiance produced by polarization effects. A semiempirical expression for this term, determined with the theory of successive order of scattering, was tested at $\lambda = 0.35$ μm for homogeneous atmospheres with τ_A (0.35 μm) ≤ 0.5 and was shown to reduce the error within ~0.6%. This theory was incorporated into the SKYRAD.pack code.

From the behavior of both simulated and measured $R(\Theta)$ and $\tau_A(\lambda)$ data at the wavelengths considered in this paper, it was deemed that some wavelengths are redundant, and that possibly their number could be reduced when the same accuracy of the result is retained.[15,62–65] To investigate this point, with the SKYRAD.pack code we computed the optical quantities for three cases of a turbid atmosphere, two refractive indices ($\tilde{m} = 1.48–0.055i$ and $\tilde{m} = 1.50–0.01i$, independent of wavelength), two retrieval modes (INDM = 2, 0), for the $3° \leq \Theta \leq 30°$ interval, and the six standard wavelengths; for each case the features of the aerosol were retrieved by the use of several combinations of wavelengths. Results showed that the accuracy of quantities R, τ_A,

and $v(r)$, reconstructed at all six considered wavelengths by the use of data at only the 0.369-μm and 1.048-μm wavelengths, is almost the same as that obtained with data from all six wavelengths.

The explanation of these results lies in the behavior of the kernel functions for scattering and extinction defined in Eq. (7). If we take into account that for $3° \leq \Theta \leq 30°$ the information content is approximately within the interval $l \leq x \leq 60$ for scattering and $0.7 \leq x \leq 20$ for extinction, one can see that the two wavelengths 0.369 and 1.048 μm cover the same radius interval as the six considered wavelengths, that is, approximately the interval $0.05 \leq r \leq 10$ μm, which was shown to be suitable for a correct reconstruction of the aerosol optical properties.

Results from experimental data[42] taken at the standard wavelengths in Cagliari (Sardinia) confirmed these findings. However, we must note that when the above computations were made, the same values of the input parameters for both cases (two and six wavelengths) were used. In practice, these input parameters have to be found by the optical data during the data-elaboration procedure, as shown in Subsection 5.C. Very recent experience concerning the elaboration of experimental data showed that with two or three wavelengths, control parameter $\epsilon(R)$ has such irregular behavior with the input parameters that possibly these latter cannot be reliably determined, so further investigations should be carried out.

Finally, in view of a worldwide diffusion of sky radiation measurements, the problems connected with data handling and processing also have to be considered. Holben *et al.*[2] described a network in which data are transmitted through the satellite data collection system from the memory of the sky radiometer to the appropriate ground receiving station and are processed in near real time. Further improvements concern, for instance, unifying the presentation and elaboration of data, extending measurements to ships and aircrafts by use of stabilized platforms, and determining the variable measurement location by means of a global positioning system.

Part of this research was funded by the Italian National Program for Antarctic Research (PNRA). We are also grateful for technical support from Prede Company, Tokyo. E. Lo Cascio provided the figures.

References

1. T. Nakajima, M. Tanaka, and T. Yamauchi, "Retrieval of the optical properties of aerosols from aureole and extinction data," Appl. Opt. **22,** 2951–2959 (1983).
2. B. N. Holben, T. F. Eck, I. Slutsker, D. Tanré, J. P. Buiss, A. Setzer, E. Vermote, J. A. Reagan, and Y. J. Kaufman, "Multiband authomatic sun and sky scanning radiometer system for measurement of aerosol," Remote Sensing Environ. (to be published).
3. Y. J. Kaufman, "Aerosol optical thickness and atmospheric path radiance," J. Geophys. Res. **98,** 2677–2692 (1993).
4. D. Tanré, C. Devaux, M. Herman and R. Santer, "Radiative properties of desert aerosols by optical ground-based measurements at solar wavelengths," J. Geophys. Res. **93,** 14223–14231 (1988).
5. G. Tonna, T. Nakajima, and R. Rao, "Aerosol features retrieved from solar aureole data: a simulation study concerning a turbid atmosphere," Appl. Opt. **34,** 4486–4499 (1995).
6. M. Shiobara, T. Hayasaka, T. Nakajima, and M. Tanaka, "Aerosol monitoring using a scanning spectral radiometer in Sendai, Japan," J. Meteorol. Soc. Jpn. **69,** 57–70 (1991).
7. T. Nakajima, M. Tanaka, T. Hayasaka, Y. Miyake, Y. Nakanishi, and K. Sasamoto, "Airborne measurements of the optical stratification of aerosols in turbid atmospheres," Appl. Opt. **25,** 4374–4381 (1986).
8. M. Tanaka, T. Hayasada, and T. Nakajima, "Airborne measurements of optical properties of tropospheric aerosols over an urban area," J. Meteorol. Soc. Jpn. **68,** 335–344 (1990).
9. T. Hayasaka, T. Nakajima, and M. Tanaka, "The coarse particle aerosols in the free troposphere around Japan," J. Geophys. Res. **95,** 14,039–14,047 (1990).
10. K.-N. Liou, *An Introduction to Atmospheric Radiation* (Academic, New York, 1980), p. 392.
11. E. P. Shettle and R. W. Fenn, "Models for the aerosols of the lower atmosphere and the effects of humidity variations on their optical properties," AFGL Rep. TR-79-0214 (U.S. Air Force Geophysics Laboratory, Hanscom Air Force Base, Mass., 1979), p. 94.
12. K. Krishna Moorthy, P. R. Nair, and B. V. Krishna Murthy, "Size distribution of coastal aerosols: effects of local sources and sinks," J. Appl. Meteorol. **30,** 844–852 (1991).
13. C. Tomasi, E. Caroli, and V. Vitale, "Study of the relationship between Ångström's wavelength exponent and Junge particle size distribution exponent," J. Climate Appl. Meteorol. **22,** 1707–1716 (1983).
14. M. D. King, D. M. Byrne, B. M. Herman, and J. A. Reagan, "Aerosol size distributions obtained by inversion of spectral optical depth measurements," J. Atmos. Sci. **35,** 2153–2167 (1978).
15. M. A. Box and G. Viera, "Information content of aerosol remote sensing experiments: scattering versus extinction," in *Proceedings of the International Radiation Symposium 1988,* J. Lenoble and J. F. Geleyn, eds. (Deepak, Hampton, Va., 1989), p. 579.
16. N. T. O'Neill and J. R. Miller, "Combined solar aureole and solar beam extinction measurements. 1. Calibration considerations," Appl. Opt. **23,** 3691–3696 (1984).
17. G. Zibordi and K. J. Voss, "Geometrical and spectral distribution of sky radiance: comparison between simulations and field measurements," Remote Sensing Environ. **27,** 343–358 (1989).
18. K. J. Voss and G. Zibordi, "Radiometric and geometric calibration of a visible spectral electro-optic 'fisheye' camera radiance distribution system," J. Atmos. Ocean Technol. **6,** 652–662 (1989).
19. T. Nakajima and M. Tanaka, "Algorithms for radiative intensity calculations in moderately thick atmospheres using a truncation approximation," J. Quant. Spectrosc. Radiat. Transfer **40,** 51–69 (1988).
20. M. A. Box and A. Deepak, "Single and multiple scattering contributions to circumsolar radiation," Appl. Opt. **17,** 3794–3797 (1978).
21. K. Arao and M. Tanaka, "Dependence of the solar aureole upon the optical properties of aerosols and albedo of the ground surface," J. Meteorol. Soc. Jpn. **64,** 743–753 (1986).
22. J. A. Weinman, J. T. Twitty, S. R. Browning, and B. M. Herman, "Derivation of phase functions from multiply scattered sunlight transmitted through a hazy atmosphere," J. Atmos. Sci. **32,** 577–583 (1975).
23. V. V. Sobolev, *Light Scattering in Planetary Atmospheres* (Pergamon, New York, 1975).

24. M. A. Box and A. Deepak, "An approximation to multiple scattering in the Earth's atmosphere: almucantar radiance formulation," J. Atmos. Sci. **38,** 1037–1048 (1981).
25. W. J. Wiscombe, "The delta-M method: Rapid yet accurate radiative flux calculations for strongly asymmetric phase functions," J. Atmos. Sci. **34,** 1408–1422 (1977).
26. T. Nakajima and M. Tanaka, "Matrix formulations for the transfer of solar radiation in a plane-parallel scattering atmosphere," J. Quant. Spectrosc. Radiat. Transfer **35,** 13–21 (1986).
27. H. C. van de Hulst, *Multiple Light Scattering, Tables, Formulas, and Applications* (Academic, New York, 1980), Vols. 1 and 2.
28. K. Stamnes and H. Dale, "A new look at the discrete ordinate method for radiative transfer calculations in anisotropically scattering atmospheres. II: intensity computations," J. Atmos. Sci. **38,** 2696–2706 (1981).
29. S. Twomey, *Introduction to the Mathematics of Inversion in Remote Sensing and Indirect Measurements* (Elsevier, New York, 1977).
30. R. Hitzenberger and R. Rizzi, "Retrieved and measured aerosol mass size distributions: a comparison," Appl. Opt. **25,** 546–553 (1986).
31. E. Trakhovsky and E. P. Shettle, "Improved inversion procedure for the retrieval of aerosol size distributions using aureole measurements," J. Opt. Soc. Am. A **2,** 2054–2060 (1985).
32. G. E. Shaw, "Inversion of optical scattering and spectral extinction measurements to recover aerosol size spectra," Appl. Opt. **18,** 988–993 (1979).
33. M. D. King, "Sensitivity of constrained linear inversions to the selection of the Lagrange multiplier," J. Atmos. Sci. **39,** 1356–1369 (1982).
34. R. Rizzi, R. Guzzi, and R. Legnani, "Aerosol size spectra from spectral extinction data: the use of a linear inversion method," Appl. Opt. **21,** 1578–1587 (1982).
35. M. Tanaka, T. Nakajima, and T. Takamura, "Simultaneous determination of complex refractive index and size distribution of airborne and water-suspended particles from light scattering measurements," J. Meteorol. Soc. Jpn. **60,** 1259–1272 (1982).
36. C. Tomasi, F. Prodi, M. Sentimenti, and G. Cesari, "Multiwavelength sun-photometers for accurate measurements of atmospheric extinction in the visible and near-IR spectral range," Appl. Opt. **22,** 622–630 (1983).
37. H. Kremser, P. Koepke, and H. Quenzel, "Aerosol optical thickness from direct solar radiation improved Langley method applied to measured data," in *Proceedings of the International Radiation Symposium 1984: Current Problems in Atmospheric Radiation,* G. Fiocco, ed. (Deepak, Hampton, Va., 1984), p. 46.
38. G. E. Shaw, "Error analysis of multi-wavelength sun photometry," Pure Appl. Geophys. **114,** 1–14 (1976).
39. M. Tanaka, T. Nakajima, and M. Shiobara, "Calibration of a sunphotometer by simultaneous measurements of direct-solar and circumsolar radiations," Appl. Opt. **25,** 1170–1176 (1986).
40. Y. J. Kaufman, A. Gitelson, A. Karnieli, E. Ganor, R. S. Fraser, T. Nakajima, S. Mattoo, and B. N. Holben, "Size distribution and scattering phase function of aerosol particles retrieved from sky brightness measurements," J. Geophys. Res. **99,** 10341–10356 (1994).
41. Y. J. Kaufman, B. N. Holben, L. Remer, A. Gitelson, A. Karnieli, and T. Nakajima, "Measurements of the ambient aerosol backscattering fraction," in *Abstracts of the Fourth International Aerosol Conference, UCLA* (University of California, Los Angeles, Calif., 1994).
42. G. Dalu, R. Rao, A. Pompei, P. Boi, G. Tonna, and B. Olivieri, "Aerosol optical properties retrieved from solar aureole measurements over Southern Sardinia," J. Geophys. Res. **100,** 864–871 (1995).
43. M. D. King and B. M. Herman, "Determination of the ground albedo and the index of absorption of atmospheric particulates by remote sensing. Part I: theory," J. Atmos. Sci. **36,** 163–173 (1979).
44. M. D. King, "Determination of the ground albedo and the index of absorption of atmospheric particulates by remote sensing. Part II: application," J. Atmos. Sci. **36,** 1072–1083 (1979).
45. F. Cabot, G. Dedieu, and P. M. Maisongrande, "Surface albedo from space over Hapex Sahel sites," in *Proceedings of the 6th AVHRR Data Users' Meeting* (European Organization for the Exploitation of Meteorological Satellites, Darmstadt, Germany, 1993), p. 51.
46. G. Hänel, "Single scattering albedo, asymmetry parameter, apparent refractive index, and apparent soot content of dry atmospheric particles," Appl. Opt. **27,** 2287–2295 (1988).
47. J. A. Reagan, K. J. Thome, and B. M. Herman, "A simple instrument and technique for measuring columnar water vapor via near-IR differential solar transmission measurements," IEEE Trans. Geosci. Remote Sensing **30,** 825–831 (1992).
48. J. Heintzenberg and R. M. Welch, "Retrieval of aerosol size distribution from angular scattering functions: effects of particle composition and shape," Appl. Opt. **21,** 822–830 (1982).
49. S. Asano and M. Sato, "Light scattering by randomly oriented spheroidal particles," Appl. Opt. **19,** 962–974 (1980).
50. A. Mugnai and W. J. Wiscombe, "Scattering from nonspherical Chebyshev particles. 3: variability in angular scattering patterns," Appl. Opt. **28,** 3061–3073 (1989).
51. M. I. Mishchenko and L. D. Travis, "Light scattering by polydispersions of randomly oriented spheroids with sizes comparable to wavelengths of observation," Appl. Opt. **33,** 7206–7225 (1994).
52. W. J. Wiscombe, "Improved Mie scattering algorithms," Appl. Opt. **19,** 1505–1509 (1980).
53. J. B. Pollack and J. N. Cuzzi, "Scattering by nonspherical particles of size comparable to a wavelength: a new semi-empirical theory and its application to tropospheric aerosols," J. Atmos. Sci. **37,** 868–881 (1980).
54. T. Nakajima, M. Tanaka, M. Yamano, M. Shiobara, K. Arao, and Y. Nakanishi, "Aerosol optical characteristics in the yellow sand events observed in May, 1982 in Nagasaki—Part II, models," J. Meteorol. Soc. Jpn. **67,** 279–291 (1989).
55. K. Arao and M. Tanaka, "Photometric and colorimetric properties of the solar aureole," J. Meteorol. Soc. Jpn. **66,** 167–177 (1988).
56. C. Tomasi, V. Vitale, and G. Zibordi, "Antarctic sky diffuse radiance in sun-photometric measurements," in *Proceedings of the Third Workshop Italian Research on Antarctic Atmosphere,* M. Colacino, G. Giovannelli, and L. Stefanutti, eds. (SIF, Bologna, Italy, 1990), p. 105.
57. M. Shiobara and S. Asano, "Estimation of cirrus optical thickness from sun photometer measurements," J. Appl. Meteorol. **33,** 672–681 (1994).
58. T. Nakajima, T. Hayasaka, A. Higurashi, G. Hashida, N. Moharram-Nejad, Y. Najafi, and H. Valavi, " Aerosol optical properties in the Iranian region obtained by ground-based solar radiation measurements in the Summer of 1991," J. Appl. Meteorol. (to be published).
59. M. A. Box and A. Deepak, "Atmospheric scattering corrections to solar radiometry," Appl. Opt. **18,** 1941–1949 (1979).
60. M. Tanaka, "Radiative transfer in turbid atmospheres. II. Angular distribution of intensity of the solar radiation dif-

fusely reflected and transmitted by turbid atmospheres," J. Meteorol. Soc. Jpn. **49,** 321–332 (1971).
61. H. Ogawa, M. Tanaka, and T. Nakajima, "A simple expression for the additional sky radiance produced by polarization effects," J. Meteorol. Soc. Jpn. **67,** 877–888 (1989).
62. S. Twomey and H. B. Howell, "Some aspects of the optical estimation of microstructure in fog and cloud," Appl. Opt. **6,** 2125–2131 (1967).
63. S. Twomey, "Information content in remote sensing," Appl. Opt. **13,** 942–945 (1974).
64. E. Thomalla and H. Quenzel, "Information content of aerosol optical properties with respect to their size distribution," Appl. Opt. **21,** 3170–3177 (1982).
65. N. T. O'Neill and J. R. Miller, "Constrained linear inversion of optical scattering data for particle size spectra: an approach to angular optimization," Appl. Opt. **21,** 1231–1235 (1982).